จุฬาลงกรณ์มหาวิทยาลัย

ทุนวิจัย

กองทุนรัชดาภิเษกสมโภช

รายงานวิจัย

การขึ้นรูปแคลเซียมฟอตเฟสชนิดพรุน

โดย

สุพัตรา จินาวัฒน์

เมษายน 2545

จุฬาลงกรณ์มหาวิทยาลัย

ทุนวิจัย

กองทุนรัชดาภิเษกสมโภช

รายงานวิจัย
การขึ้นรูปแคลเซียมฟอสเฟตชนิดพรุน

โดย
สุพัตรา จินาวัฒน์

เมษายน 2545

Chulalongkorn University

Research Grant

Ratchadaphiseksomphot Endowment

Fabrication of Porous Calcium Phosphates

BY

Supatra Jinawath

April 2002

ชื่อโครงการ	การขึ้นรูปแคลเซียมฟอสเฟตชนิดพรุน
ผู้วิจัย	สุพัตรา จินาวัฒน์
เดือนและปีที่ทำวิจัยเสร็จ	เมษายน 2545

บทคัดย่อ

การขึ้นรูปแคลเซียมฟอสเฟตชนิดพรุน

สารตั้งต้นที่ใช้สำหรับงานวิจัยเรื่องนี้ได้แก่ โมโนแคลเซียม ฟอสเฟต โมโนไฮเดรต ไดแคลเซียม ฟอสเฟต ไดไฮเดรต และ แอนไฮดรัส ไดแคลเซียม ฟอสเฟต สังเคราะห์จากวัสดุผลพลอยได้ของอุตสาหกรรมการผลิตเจลาตินจากกระดูกสัตว์ในประเทศ ได้ทำการผลิตแคลเซียมฟอสเฟตชนิดพรุน ซึ่งมีองค์ประกอบเป็น ไฮดรอกซีอพาไทท์ ทั้งในรูปเฟสเดี่ยวหรือในรูปเชิงประกอบร่วมกับสารในเครือ เช่น เบตาไตรแคลเซียมฟอสเฟต (β-TCP) ในสภาพเป็นเม็ด (granules) และเป็นชิ้น (compacts) ลักษณะเฉพาะของชิ้นตัวอย่างที่เด่น มีความพรุนร้อยละ 37 โดยปริมาตร มีลักษณะของรูพรุนที่ต่อเนื่อง ขนาดเส้นผ่านศูนย์กลาง 1-30 ไมโครเมตร ชิ้นงานมีความแข็งแรงดัด และความแข็งแรงกดเท่ากับ 17.51 และ 78.13 เมกะปาสคาล ตามลำดับ ในการทดลองนี้ยังได้ทำการศึกษาตัวแปรต่างที่มีผลต่อสมบัติของผลิตภัณฑ์ที่ได้ด้วย นอกจากนี้ยังสัมฤทธิ์ผลในการเปลี่ยนปะการังเป็น ไฮดรอกซีอพาไทท์ ที่ยังคงขนาดรูพรุนเดิม (200μm) ไว้ได้

Project Title: FABRICATION OF POROUS CALCIUM PHOSPHATES

Name of the Investigator: Supatra Jinawath

Year: April 2002

ABSTRACT

Fabrication of Porous Calcium Phosphates

The starting materials for this experiment were monocalcium phosphate monohydrate, dicalcium phosphate dihydrate and anhydrous dicalcium phosphate synthesized in-house from the by-product of a local bone-gelatin manufacture. Porous calcium phosphates comprising hydroxyapatite either as a single phase or a composite containing traces of its congeners, i.e., β-TCP were fabricated in the forms of granules and compacts. The characteristics of typical compacts produced were 37 v % apparent porosity with interconnected pores of diameter 1-30 μm, and flexural and compressive strengths of 17.51 and 78.13 MPa, respectively. Effects of fabrication parameters on the properties of the products were also studied. In addition, coralline hydroxyapatite-converted coral with preservation of its 200-μm-pore architecture, was also successfully produced.

Keywords: Coralline hydroxyapatite, hydrothermal synthesis, porous calcium phosphates

Acknowledgements

The author would like to express her gratitude to the Rachadapiseksomphot Endowment, Chulalongkorn University, for the financial support, and her sincere thanks to Ms. P. Sujaridworakun and Ms. D. Polchai for the experimental work, and Mr. W. Prakaypun for manuscript preparation. Without whom mentioned, this task can never be accomplished.

Contents

List of Tables

List of Figures

Chapter 1

Introduction

Calcium phosphates having respective Ca/P mole ratios of 0.5 to 2 have been successfully synthesized in our laboratory, formerly from bovine bone ash, and recently from the by-product of bone-gelatin industry with the advantage over the former one in that the bone preparation step which includes cleaning, calcining and grinding of the bone is completely eliminated and so is the bad smell in the calcining process.[1,2,6] In this work, dicalcium phosphate dihydrate (DCPD) and dicalcium phosphate anhydrous (DCPA) synthesized from the mentioned by-product were used as the starting materials for the fabrication of porous calcium phosphate ceramics - hydroxyapatite (HA) and β- tricalcium phosphate (β -TCP).

Typical applications of medical grade hydroxyapatite are dense blocks, macroporous blocks and granules (~ 60% porosity), for bone grafting, augmentation, infilling and preforms that the surgeon will shape during surgery. However, each of the block form has its drawbacks, poor machinability of the dense HA and the ragged surface finish of the macroporous material. Recently, a hydroxyapatite ceramic with micro to mesoporosity rendering a better machinability has been reported[3] which has lit up the purpose of this study since it means that higher strength can be reached with this range of pore size. It is also quite possible that macropore may not be necessary for resorbable and porous material because after implantation it will be gradually degraded . Although it has been known that degradation rate of hydroxyapatite ceramic depended greatly on its mineral phase, (Ca/P mole ratio). However, nature of porous structure, to a certain extent, can be another factor. Hence, a micro to mesoporous ceramic having an appreciable strength and machinability with appropriate retention time for conducting bone tissue in the body may be an ideal implant. Moreover, with the enhancement of fabrication technology, porous ceramics with controlled morphology and porosity are possible.[4,5] However, the fabrication of porous calcium phosphate ceramic, especially hydroxyapatite and β-tricalcium phosphate for medical application, is complicated

since it needs not only biocompatibility but also an appropriate combination between pore size and strength. Hence a further research has to be attempted.

The objective of this project is to produce porous HA or β-TCP bioceramic with high strength and appreciable machinability from available natural sources (bovine bone or by-product from related industries) with our own technology. The next step is to co-operate with medical people for in vivo experiment, i.e. as bone filling, dental preform for glass-infiltration and eye socket support. It is hoped that the material will benefit our social services.

Chapter 2

Theory

Calcium phosphates of medical interest are hydroxyapatite (HA) and β-tricalcium phosphate (β-TCP). They have been increasingly used as bone filling and bone substitution[6,7,8] with a better bicompatibility than that of the other ceramic implants. However, due to the poor mechanical property, their viability is restricted to non-load bearing applications. Porous calcium phosphate ceramics have been reported to form a strong bond to the bone, enhancing fixation and conducting bone tissue into the pores[9]. Moreover, they are resorbable[6,7,8] hence they can be progressively replaced by natural bone tissue.

2 methods to fabricate porous ceramics :[5,10,11,12]

1. Using a preform

A polymeric sponge is dipped in the prepared ceramic slurry. Then it is calcined to get rid of the sponge and followed by sintering to a rigid mass. The other way is mixing the granules of some organic or polymeric materials with ceramic powder which after shaping, calcining and sintering, the granules will create a porous structure. The size of the pores as well as their interconnection directly depends on the nature of the preform.

2. Foaming method

Normally chemicals able to give gases after reaction, such as H_2O_2 , paraffin, naphthalene and etc. are employed in the ceramic slurry or in the pressing powder.

The 1st method gives only interconnected pore structure while the 2nd method is capable of producing either interconnected or close porosities. Pore size and distribution ranging from micro (< 5μm) to macropore (>150 μm typical diameter) can be obtained by these methods.

Chapter 3

Experiment

3.1 Materials

- **Chemicals**
  - HNO_3 acid (69.0-70.0%, Actual analysis, J.T. Baker)
  - H_3PO_4 acid (85%, BDH AnalaR)
  - NH_4OH sol. (35% NH_3, BDH AnalaR)
  - Acetone (Actual Analysis. J.T. Baker)
  - $CaCO_3$ (>99%, Fluka)
  - H_2O_2 solution (35%)
  - Dispex N40 (Ammonium salt of polycarboxylic acid solution)
  - Polyvinylpyroridone (PVP powder, MW 40,000)
  - Polyvinylalcohol (PVA powder, MW 115,000, degree of hydrolysis 87%, BDH)
  - Calcium Stearate (Powder Formosa Organic Chemical Industry Co.,Ltd)
  - Polyethylene glycol (PEG granule, MW 4000) and PEG 200 (solution, Merck-Schuchardt)
  - Monocalcium phosphate monohydrate powder, MCPM ($Ca(H_2PO_4)_2.H_2O$, Riedel-de-Haen AG)

- **Starting materials**

The starting materials are DCPD ($CaHPO_4.2H_2O$), DCPA ($CaHPO_4$) and MCPM ($Ca(H_2PO_4)_2.H_2O$) synthesized from by-product of bone-gelatin manufacture in our laboratory.

The main reactions taking place during sintering :

$$6\ CaHPO_4.2H_2O + 4CaCO_3 \xrightarrow{1100\text{-}1200^{\circ}C} Ca_{10}(PO_4)_6(OH)_2 + 4CO_2 + 14H_2O \quad \ldots. (1)$$

$$6\ CaHPO_4 + 4CaCO_3 \xrightarrow{1100\text{-}1200^{\circ}C} Ca_{10}(PO_4)_6(OH)_2 + 4CO_2 + 2\ H_2O \ldots\ldots (2)$$

$$3Ca(H_2PO_4)_2.H_2O + 7Ca^{2+} \xrightarrow{160\text{-}200^{\circ}C} Ca_{10}(PO_4)_6(OH)_2 + H_2O + 7H_2 \quad \ldots\ldots (3)$$

Ca^{2-} is from soluble calcium salts (e.g. Ca citrate, Ca-nitrate, etc)

3.2 Method[11,13,14]

To achieve a porous specimen with high strength, the specimen must have an appreciable sintered density as well as a controlled porosity. Densification can be done by many means provided that there is no resulting effect on the biocompatibility of the densified product. The following methods of fabrication are chosen for this experiment.

1. Casting a well dispersed calcium phosphate slip with 10 v % H_2O_2 foaming agent. The fine particle size of solid dispersed has to be appropriately graded to give a dense packing.
2. Pressing a well dispersed calcium phosphate powder with some chemicals to give gases after reaction ($CaCO_3$ as mesopore former) and some polymer sphere (polyethylene glycol (PEG) as macropore former) , then densifying by adding sintering aids, i.e. glass or fluxing agents.

Pressing theory

One technique to achieve a high strength specimen from powders is through a combination of granulation and dry pressing. The fine powder is first made into granules of appropriate sizes and flow properties (40-200 μm and < 5 wt % 20 μm) before they are uniaxially pressed into a die using either single or double-action press modes. Stages in dry pressing include (1) the filling of the die (2) compaction and shaping, and (3) ejection. The maximum pressing pressure used in dry pressing is commonly in the range of 20-100 MPa; higher pressures are used for technical ceramics than for clay-based materials. The most common defects in dry-pressed compacts are laminations, cracks and density variation. Controlled factors in dry pressing are as follows:

1. Die-fill density, D_{fill} (25-35 %)
2. Die wall friction
3. Packing density (high D_{press})
4. Expansion on ejection (spring back < 0.75 %)

In order to achieve a pressed specimen with high density in this experiment, granulation of the powder materials was performed as follows : DCPD (median size of agglomerate 13 μm.) and DCPA (median size of agglomerate 7 μm.) powders were each mixed with reagent grade $CaCO_3$ (median size 24 μm.) in the proportion close to the stoichiometric HA, 0-5 wt% $Ca(PO_3)_2$ glass powder (<75 μm.), 0-35 v% polyethylene glycol (PEG) granules (150-300 μm.), 1.2 wt% PVA as binder and 0.5 wt% calcium stearate as lubricant in a planetary mill. Granulation was later performed on the mixture with approximately 5-10% moisture. The free flowing granules (90 wt% 300-500 μm. and 10 wt% 105-300 μm.) were uniaxially pressed into cylinder (13 × 6.5 mm.diameter) and rectangular bar (4×4×44 mm.) using double action pressing mode. The specimens were calcined up to 550°C at a rate of 1-2 °C/min and followed by sintering for 2 h at 1200 and 1250°C at a rate of 2-3°C/min in an electric furnace. Fig. 3.1 is the firing schedule for the pressed specimens.

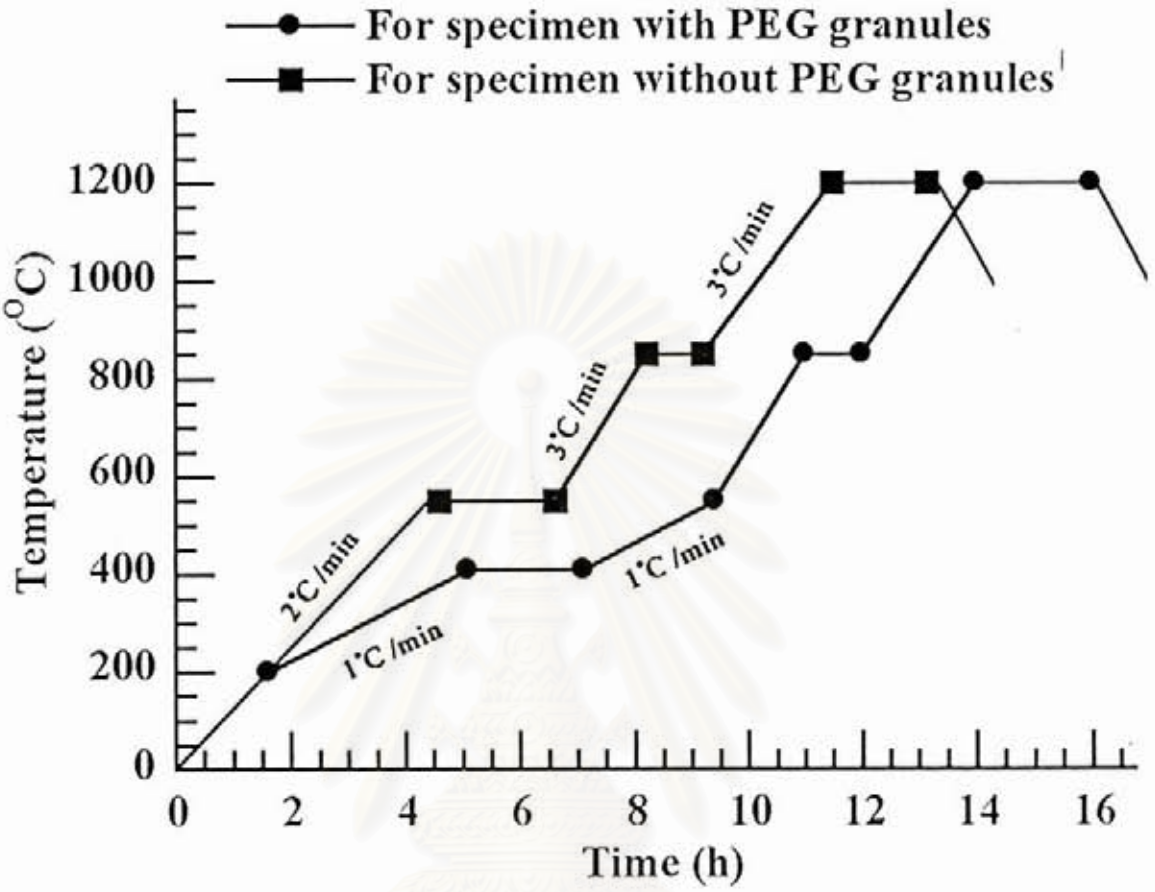

Fig. 3.1 Firing schedule for the pressed specimens.

3. Hydrothermal transforming natural coral (aragonite ($CaCO_3$)) to calcium phosphate so that the structure and strength of the coral can be retained.

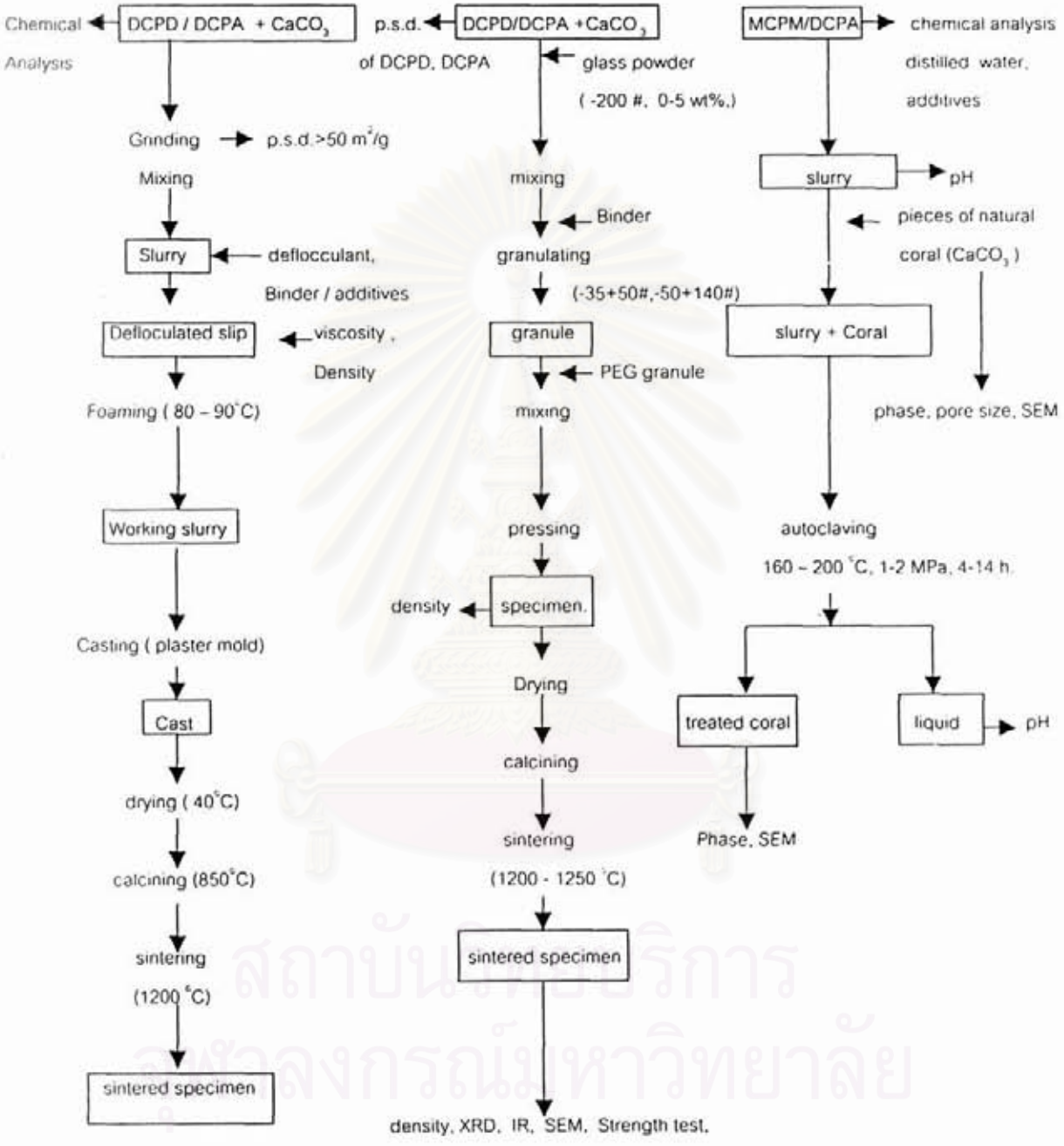

Fig. 3.2 Flow chart for the fabrication of porous calcium phosphates

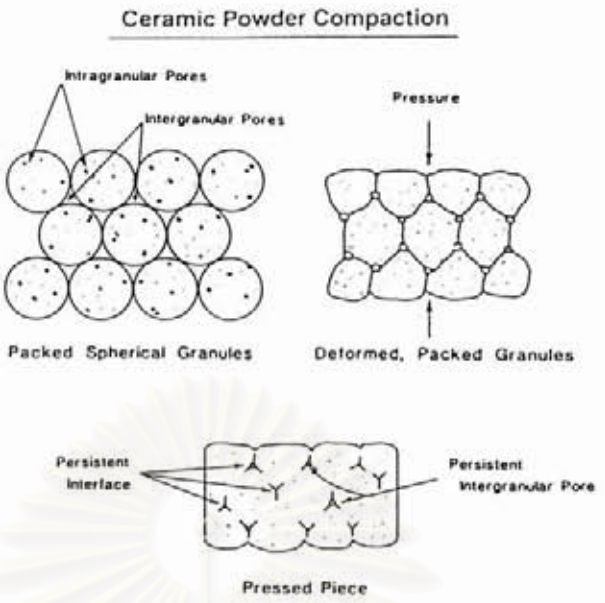

Fig. 3.3 Illustration of change in shape and change of bimodal pore size distribution during compaction.

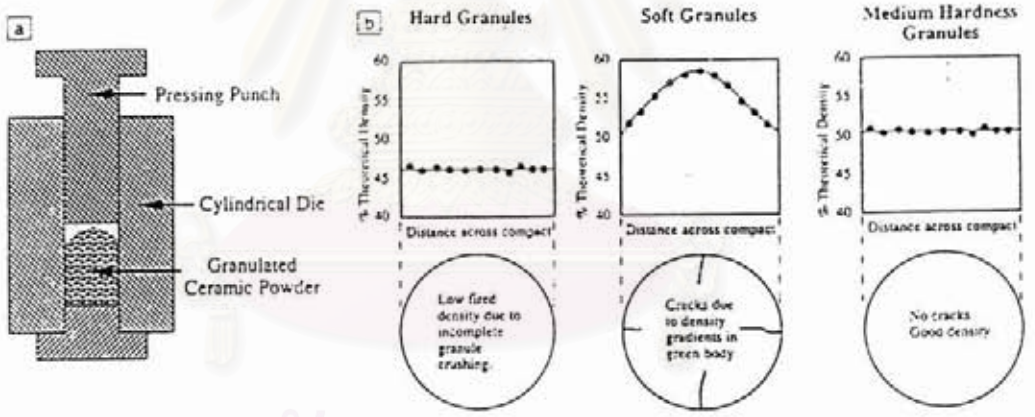

Fig. 3.4 (a) An illustration of the convex arrangement of granules used to achieve irregular die filling in Onoda's study to evaluate the effects of granule hardness on compaction and sintering. (b) qualitative results of Onoda's compaction experiments with nominally hard, soft, and medium hardness alumina granules compacted uniaxially using uneven die filling as illustrated in Fig. 4a. The upper set of graphs show density across the diameter of the as-pressed compacts. The lower set of illustrations are schematics showing the appearance of the fired pellets (top view). The best results were achieved with medium-hardness granules. Granules hardness was modified by granulating the alumina with different organic binders.

Chapter 4

Results and discussion

4.1 Starting materials and their characterization

- By-product of bone – gelatin manufacture

Fig. 4.1 and 4.2 show the XRD pattern and the FT-IR spectrum of the light brown Powder, respectively. The XRD shows that it is composed of DCPD and a trace of DCPA. The FT-IR spectrum reveals a trace of CO_3^{2-} incorporated in the lattice at 1400-1500 cm^{-1}. Its bar-like crystals in various sizes are shown in Fig 4.3. The typical size is about $1\frac{1}{2} \times 2\frac{1}{2} \times 10$ μm.

- $CaCO_3$

Fig 4.4 is the prismatic, rhombohedral crystals of $CaCO_3$ with the particle size ranging from 3 – 40 μm and the average particle size of 24 μm (Fig. 4.5).

- Synthesized DCPD

A single phase of DCPD is shown in the XRD pattern (Fig. 4.6) and a small quantity of CO_3^{2-} is also present (Fig. 4.7). The chemical analysis (by ICP) shows traces of impurity and the molar ratio of Ca/P equal to 1.13 which is slightly above the stoichiometric value of 1.00. The micrographs of DCPD in Fig. 12 showing bar-like crystals resulted from the aggromeration of the plate-like which are disintegrated after dispersion.

- Synthesized DCPA

As shown in the XRD pattern (Fig. 4.8), a single phase DCPA is obtained. Traces of impurity (by ICP) are comparable to those of DCPD but with a higher Ca/P molar ratio of 1.21. This may be due to the higher CO_3^{2-} content in its lattice, revealed by the FT-IR spectrum (Fig. 4.9).

Fig. 4.10 is the SEM images of DCPA showing the agglomerates of the prismatic DCPA crystals and the dispersed one. It is seen that the actual crystal is very small

having diameter of ~ 1 μm. The value of the average particle size of DCPA obtained from the centrifugal particle size analyzer (Shimudzu SA-C-P2, Fig.11) is about 7 μm which obviously belongs to the agglomerate. Fig. 4.12 also shows the agglomerates of DCPD crystals and the discrete crystals of which the actual size is ~ 2-3 μm. The average particle size of 13 μm from Fig. 4.13 is again, the size of the agglomerate which is ranging from 25-40 μm. Therefore it is very difficult to get an actual value of particle size of a very fine powder by sedimentation technique.

- Calcium metaphosphate glass ($Ca(PO_3)_2$)

Fig. 4.14 is the XRD patterns of the chemical, MCPM used in the preparation of $Ca(PO_3)_2$ glass at 1050°C, as received and after calcining at 550°C which are in accordance with the thermal transformation of monocalcium phosphate dihydrate (MCPD) presented by Aoki.[1]

- PEG granules (10 wt% of 50-140 #, 90 wt% of 35-50 # sieve)

Fig. 4.15 is the picture taken by a stereomicroscope of the spherical PEG granules, varying in size from 150-300 μm (35-50 # sieve, ASTM E 11) and Fig. 4.16 is the DTA/TG curves of the PEG granules showing the temperature of decomposition with a big weight loss around 464°C and a small exothermic peak with no weight loss at 673°C. Accordingly, the firing rate of 1 and 2°C/min was employed for burning out of the organic substances in the specimens with and without PEG from 250-550°C.

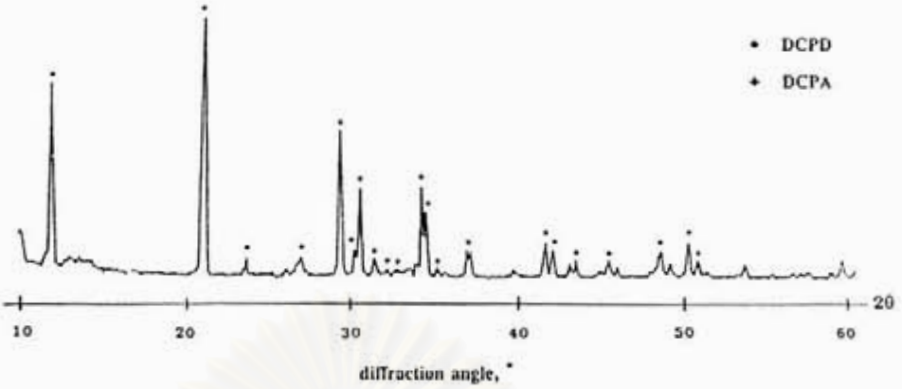

Fig. 4.1 XRD pattern of starting material (by-product).

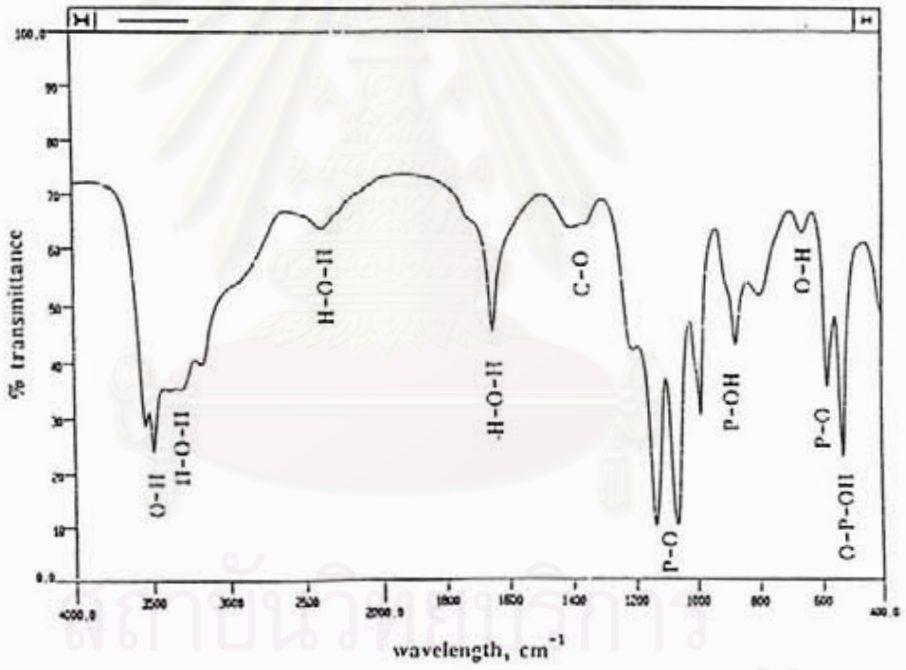

Fig. 4.2 FT-IR spectrum of starting materials.

XRD Phillip PW 1390/10

FT-IR Perkin Elmer 1760x

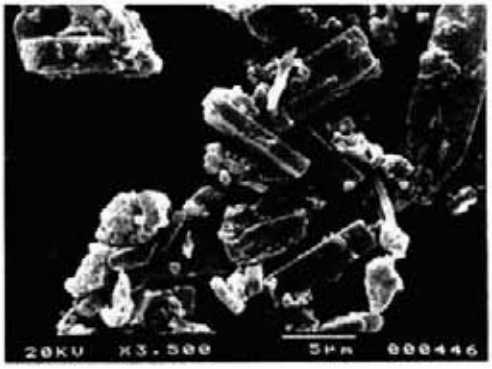

Fig. 4.3 SEM image of starting material crystals.

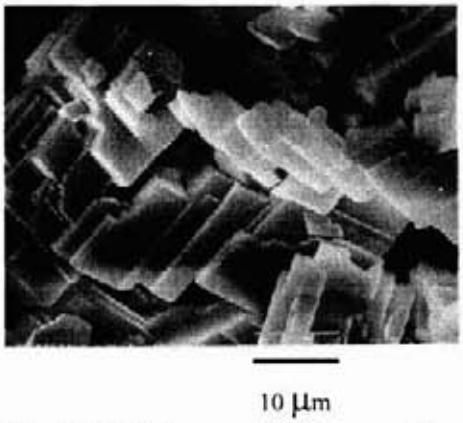

Fig. 4.4 SEM image of $CaCO_3$ crystals.

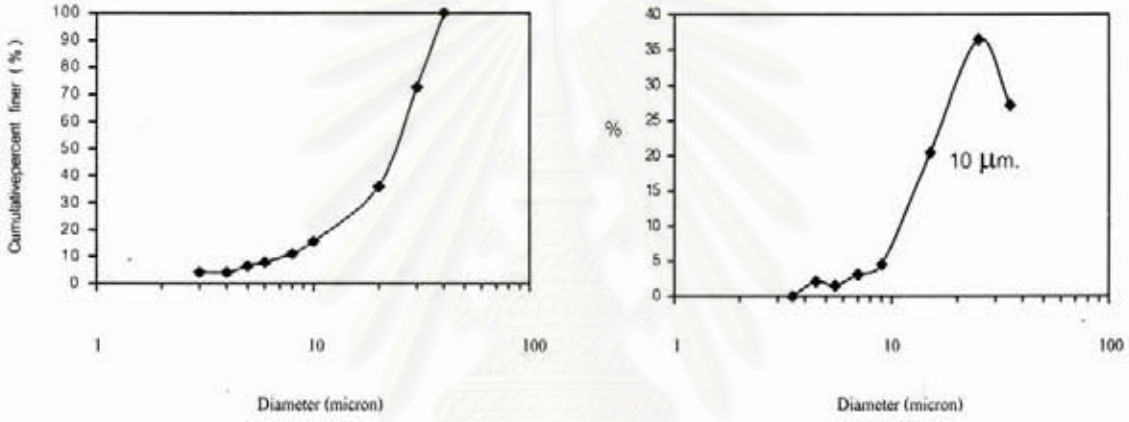

Fig. 4.5 Particle size distribution of $CaCO_3$.

SEM (JEOL : JSM-6400)
Centrifugal partical size analyzer (Shimadzu SA-CP2)

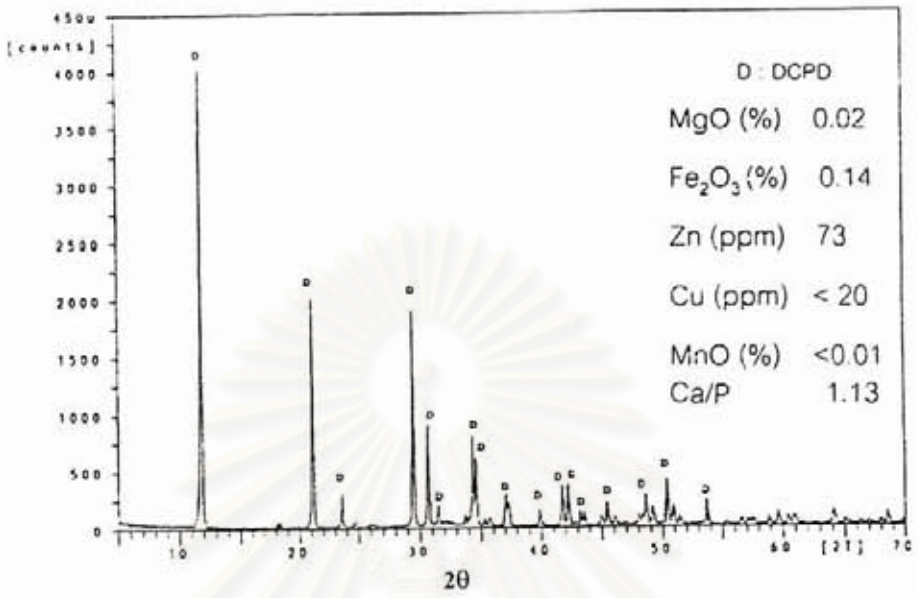

Fig. 4.6 XRD pattern of synthesized DCPD.

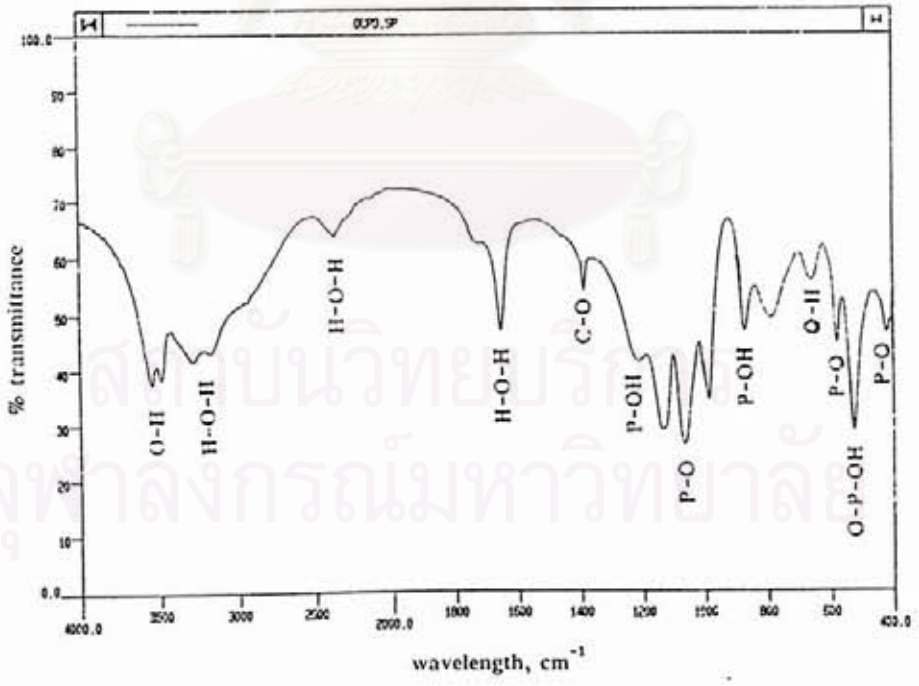

Fig. 4.7 FT-IR spectrum of synthesized DCPD.

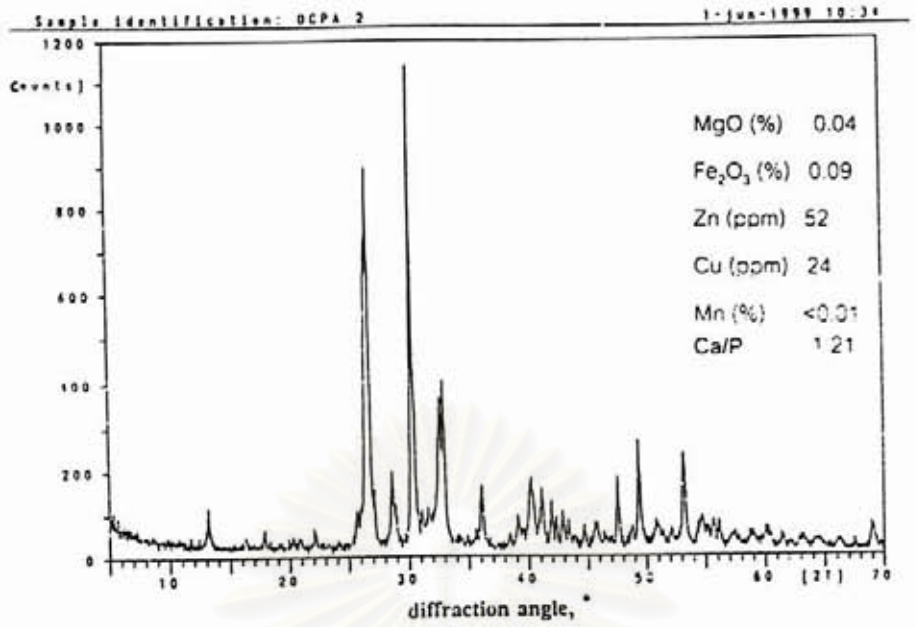

Fig. 4.8 XRD pattern of synthesized DCPA.

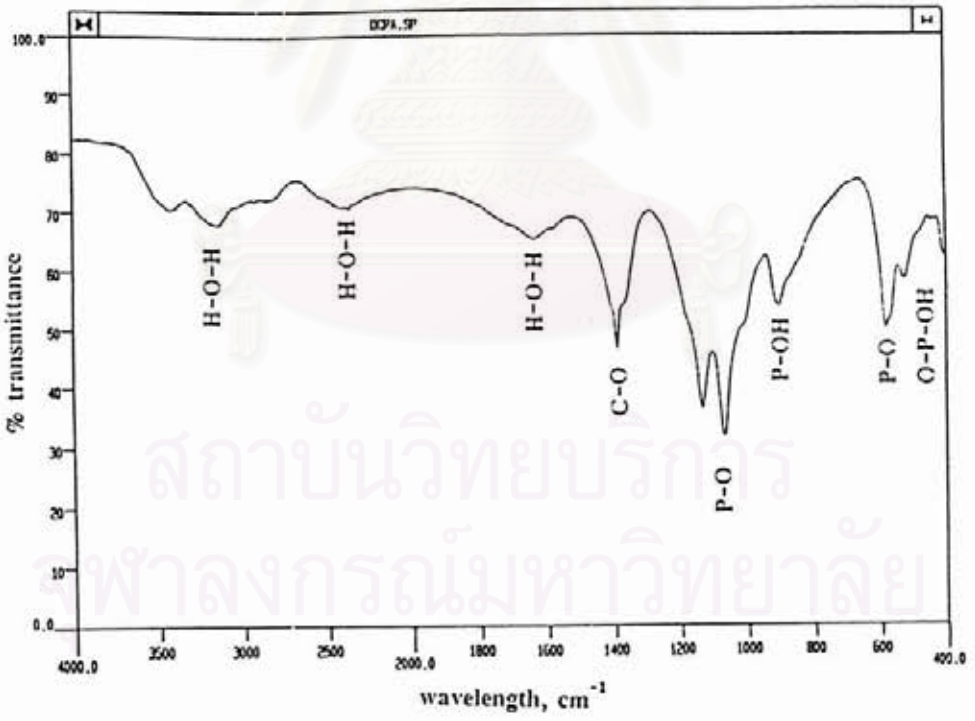

Fig. 4.9 FT-IR spectrum of synthesized DCPA.

(a) (b)

Fig. 4.10 SEM images of the agglomerates (a) and dispersed DCPA crystals (b).

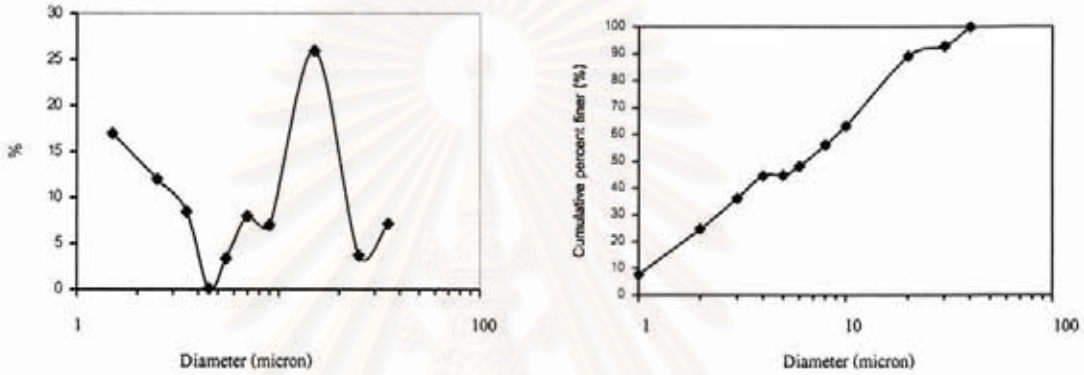

Fig. 4.11 Particle size distribution of DCPA.

(a) (b)

Fig. 4.12 SEM images of agglomerates (a) and dispersed DCPD crystals (b).

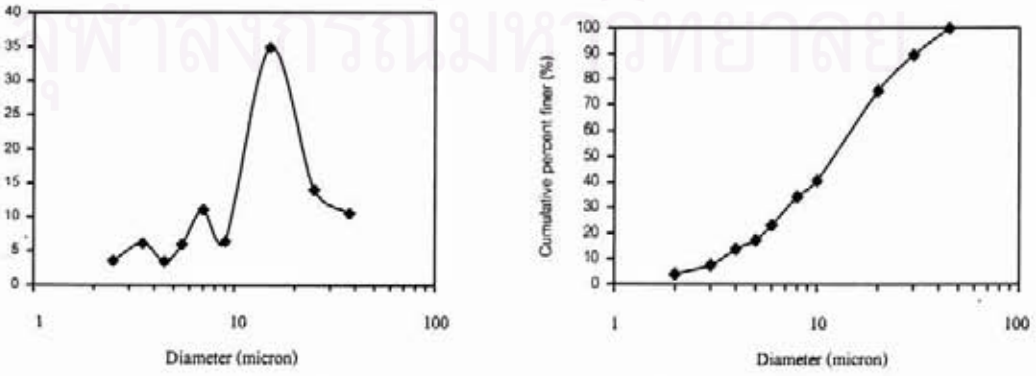

Fig. 4.13 Particle size distribution of DCPD.

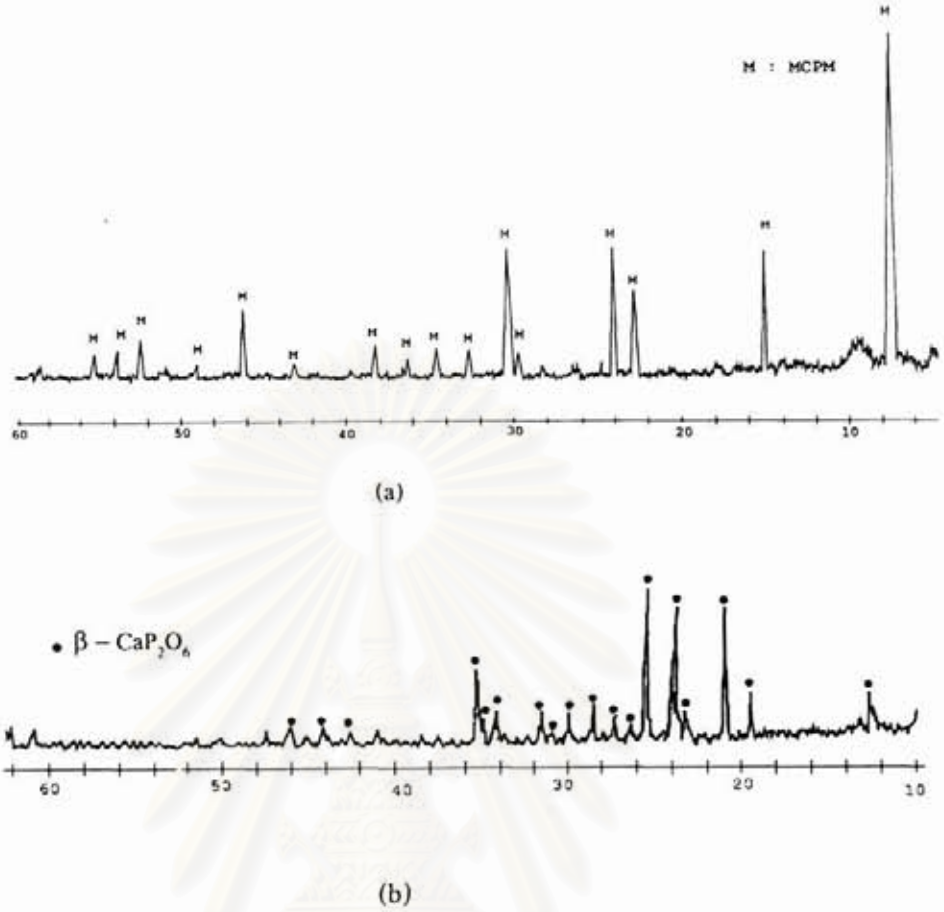

Fig. 4.14 XRD patterns of chemical MCPM as received (a) and after calcined at 550°C (b).

Thermal change of MCPD[6]

$$Ca(H_2(PO_4)_2.2H_2O \xrightarrow{250\,^{\circ}C} Ca(H_2PO_4)_2 \xrightarrow{300\,^{\circ}C} \text{amorphous } Ca(PO_3)_2 + Ca_4H_2P_6O_{20}$$

$$\xrightarrow{440\text{-}450\,^{\circ}C} \gamma\text{-}Ca(PO_3)_2 \xrightarrow{540\text{-}640\,^{\circ}C} \beta\text{-}Ca(PO_3) \xrightarrow{950\text{-}970\,^{\circ}C} \alpha\text{-}Ca(PO_3)_2$$

$$\xrightarrow{1000\,^{\circ}C} Ca(PO_3)_2 \text{ glass}$$

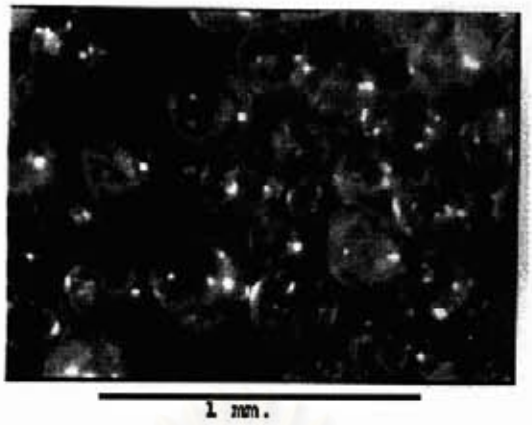

Fig. 4.15 The spherical PEG granules (stereo microscope).

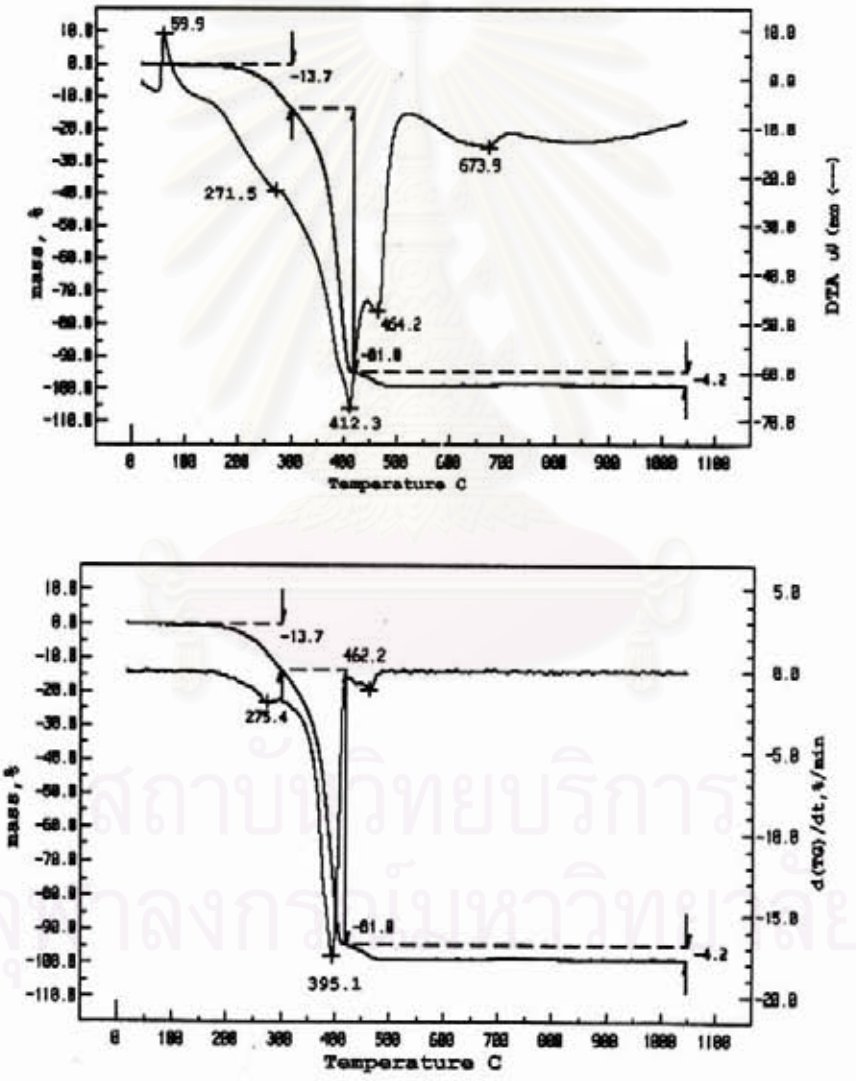

Fig. 4.16 DTA/TG curves of PEG granules.

DTA, TG (Netzch STA 409)

4.2 Calcium phosphate products

There are 3 types of porous calcium phosphate products produced in this experiment : HA granules, HA compacts fabricated by slip casting and by pressing and coralline hydroxyapatite.

4.2.1. HA granules

Fig. 4.17 is the picture taken by a stereomicroscope, showing the irregular surface of the rounded DCPD granules of 300-500 μm fraction. Table 4.1 shows the flow properties of the prepared DCPD and DCPA granules. The data clearly showed that DCPA had a better flow property which rendered it the denser microstructure after sintering at 1200°C as seen in the SEM image, Fig. 4.18. The XRD patterns in Fig. 4.19 confirmed that DCPD granule was composed of single phase HA ,and DCPA granule was HA with a trace of CaO.

4.2.2. HA compacts (slip casting)

A. Slip casting

In order to achieve the optimum fluidity of the DCPD casting slip, the defloculation behavior of the system was studied and this is shown in Fig. 4.20. The optimum defloculant needed was 0.5 wt%. The specimens sintered at 1200°C were composed of mixed phases of HA , β-TCP, α-TCP and a trace of CaO (Fig. 4.21). This suggested the segregation of slip composition brought by the big difference between the particle size of $CaCO_3$ (~24 μm) and DCPA or DCPD (1-3 μm). Moreover, the segregation was accelerated by the foaming effect of H_2O_2 which released O_2 bubbles through the surface. Therefore, compositions at 3 different depths of the specimen were investigated by XRD to confirm the above suggestion. The results from Fig. 4.22 showed that the top layer, rich in fine grains of DCPA or DCPD, was composed of β-TCP as the

main phase and HA as the minor. The middle layer was the same phase as those of the top but with a higher HA content and traces of β-TCP and CaO while the bottom layer, rich in $CaCO_3$, was mainly HA and a trace of β-TCP.

Fig. 4.23, the SEM image of the DCPD cast specimens sintered at 1200°C showed loosely sintered grains with an appreciable grain growth, micropores between sintered grains, mesopores created by the decomposition of $CaCO_3$ and macropores by foaming. The microstructures of both HA granules and DCPD cast specimens are quite similar.

From the results obtained, it was not possible to fabricate the porous cast specimen with high strength without reducing the particle size of $CaCO_3$. Since the particle size of $CaCO_3$ used was in the mesopore range hence it was the mesopore controller which should be kept. Therefore the attempt has been turned to the pressing method.

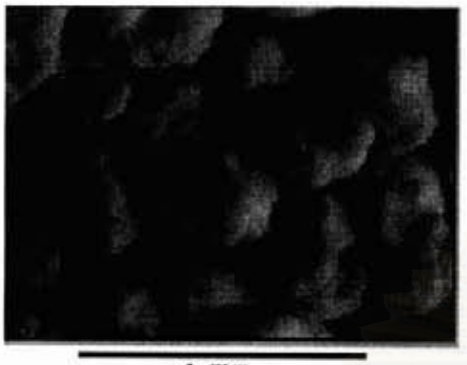

Fig. 4.17 DCPD granules (stereo microscope).

Table 4.1 Properties of the granules.

Properties	granules	
	DCPD	DCPA
Moisture (%)	5-8	9-12
Flow rate (g/sec)	0.26	0.28
Fill density (g/cm^3)	0.67	0.81
Tap density (g/cm^3)	0.83	0.93
Tap density / Fill density	1.24	1.15

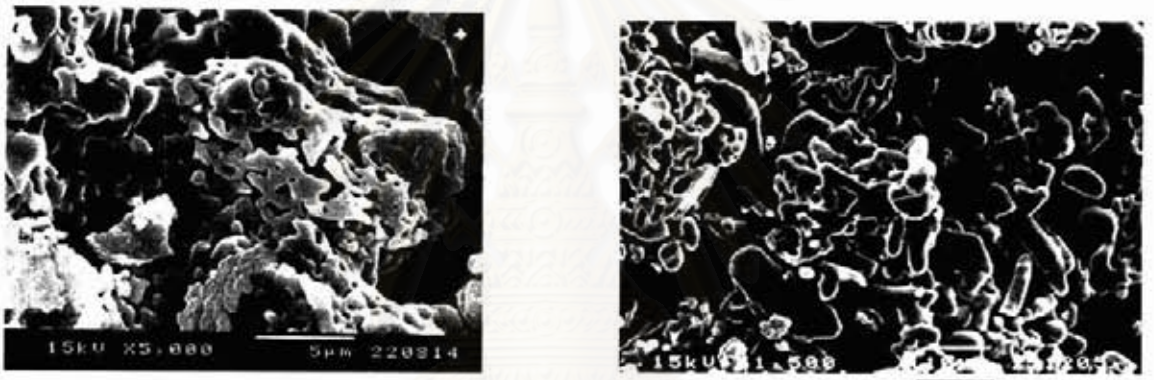

(a) (b)

Fig. 4.18 SEM images of DCPA (a) and DCPD granules (b) sintered at 1200°C.

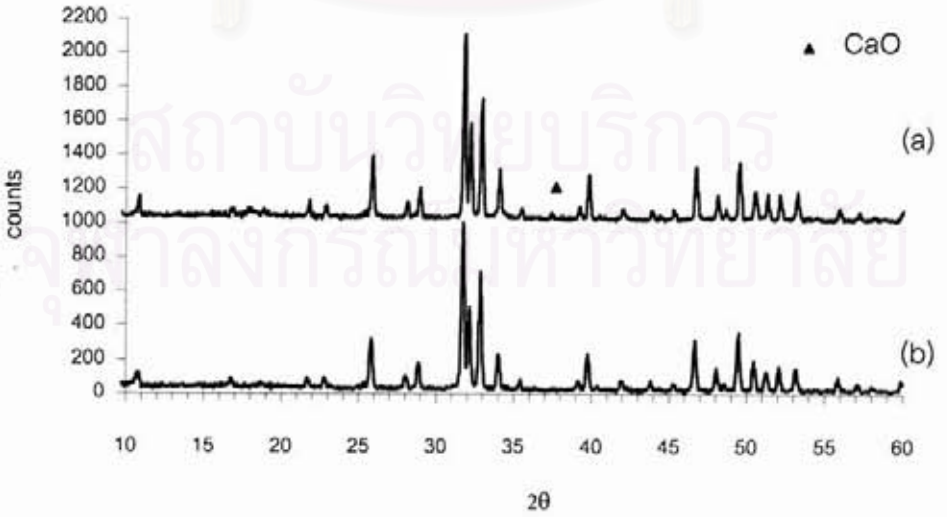

Fig. 4.19 XRD patterns of the DCPA (a) and DCPD granules (b), sintered at 1200°C.

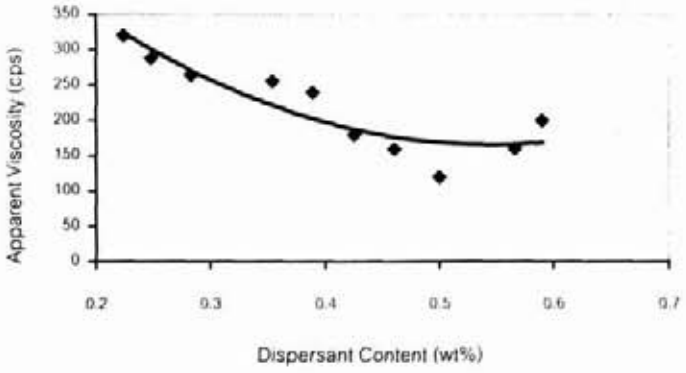

Fig. 4.20 Deflocculation curve of the DCPD + $CaCO_3$ slip.

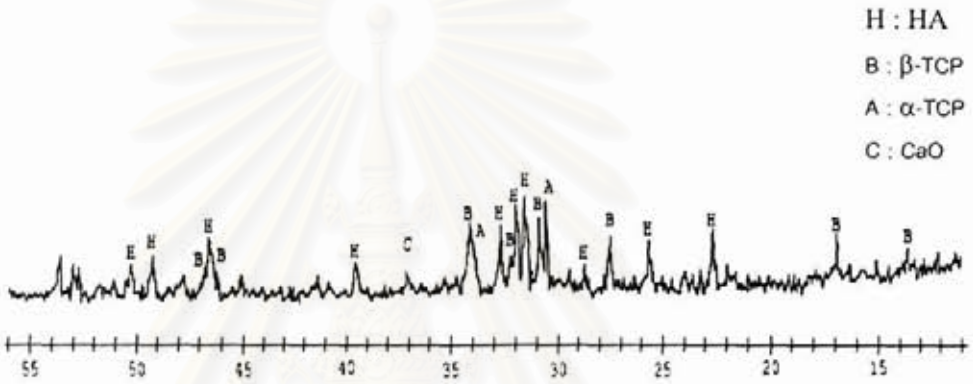

Fig. 4.21 XRD pattern of the cast sintered at 1200°C.

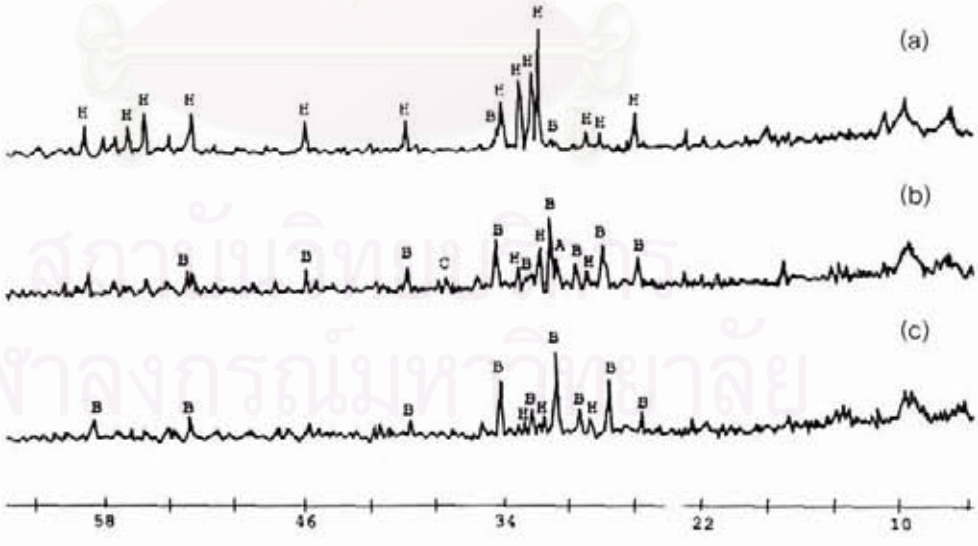

Fig. 4.22 XRD patterns of the cast at different depths : (a) bottom, (b) middle and (c) top layers.

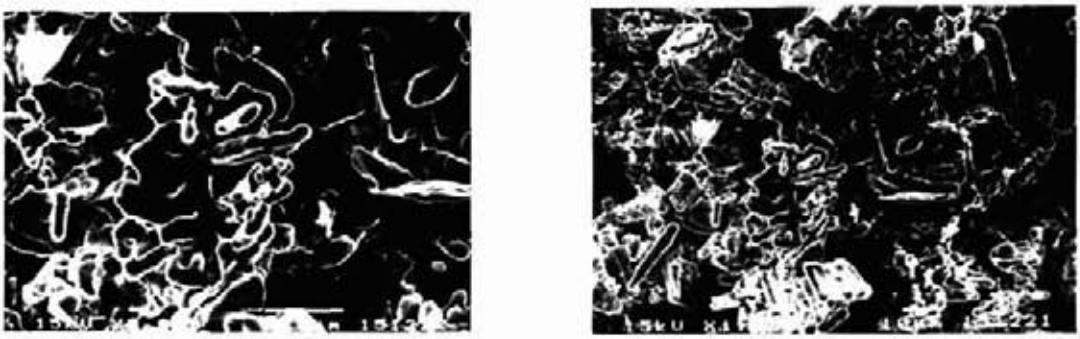

(a) Enlarged (b)

Fig. 4.23 SEM images of the cast sintered at 1200°C.

B. Pressing

The sintered specimens from pressing (Fig. 4.24) were characterized in terms of physical and mechanical properties, microstructure and phase analysis. The effects of glass (0-5 wt %), pressing pressure and sintering temperature upon the mentioned properties were also studied.

a) Compressive strength b) Flexural strength

Fig. 4.24 Specimens for mechanical testing.

- Physical and mechanical properties

Summarized results of physical and mechanical properties of the sintered specimens are tabulated in Table 4.2 and 4.3, respectively and the effect of parameters upon them are graphically presented as histograms in Fig. 4.25-4.28.

Table 4.2 Summarized results of physical properties and flexural strengths of specimens prepared from DCPD/DCPA (pressing pressure 50.1 MPa).

Sintering temperature (°C)	Physical properties	DCPD + glass			DCPA + glass		
		0 wt%	5 wt%	5 wt%+PEG	0 wt%	5 wt%	5 wt%+PEG
1200	Bulk density (g/cm^3)	1.60	1.72	1.17	1.80	1.87	1.45
	Apparent Porosity (V%)	47.35	46.60	63.72	39.87	36.17	51.49
	Flexural st.* (MPa)	8.36±0.36	8.05±0.51	2.48±0.28	15.32±1.72	15.84±0.82	3.69±0.86
1250	Bulk density (g/cm^3)	1.74	1.75	1.18	-	-	-
	Apparent Porosity (V%)	47.18	44.59	58.03	-	-	-
	Flexural st.* (MPa)	14.71±1.12	7.83±0.73	2.79±0.50	-	-	-

*Number of specimens = 5, tested at 95% confidence level.

Table 4.3 Summarized results of physical properties and compressive strengths of specimens prepared from DCPD/DCPA (pressing pressure 59 MPa).

Sintering temperature (°C)	Physical properties	DCPD + glass			DCPA + glass		
		0 wt%	5 wt%	5 wt%+PEG	0 wt%	5 wt%	5 wt%+PEG
1200	Bulk density (g/cm^3)	1.57	1.61	1.17	1.86	1.87	1.39
	Apparent Porosity (V%)	48.90	46.13	60.30	36.57	36.18	54.23
	Flexural st.* (MPa)	20.59±2.89	24.36±3.19	3.93±0.24	64.88±5.02	76.54±9.65	4.50±0.97
1250	Bulk density (g/cm^3)	1.63	1.66	1.18	-	-	-
	Apparent Porosity (V%)	45.73	41.98	59.84	-	-	-
	Compressive st.* (MPa)	21.77±1.99	27.94±2.57	4.78±0.24	-	-	-

* Number of specimens = 5, tested at 95% confidence level.

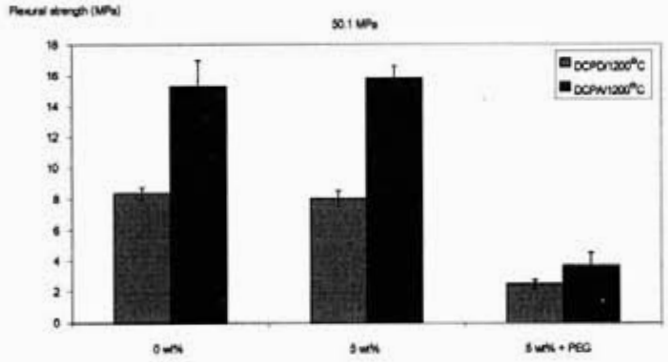

Fig. 4.25 Effect of glass on the flexural strength of specimens prepared from DCPD and DCPA.

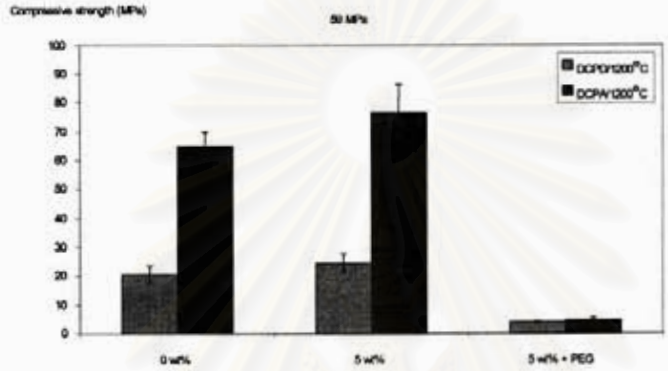

Fig. 4.26 Effect of glass on the compressive strength of specimens prepared from DCPD and DCPA.

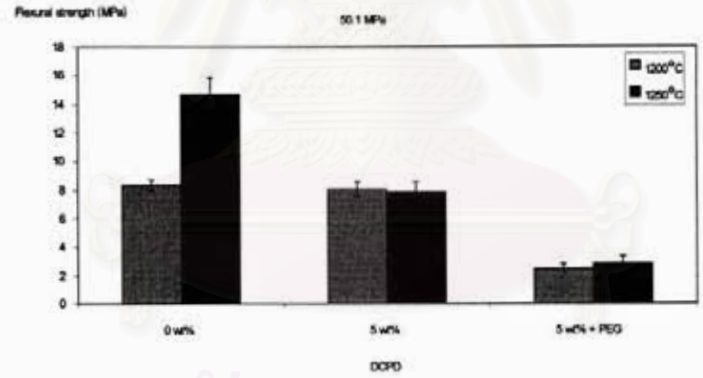

Fig. 4.27 Effect of sintering temperature on the flexural strength of specimens prepared from DCPD.

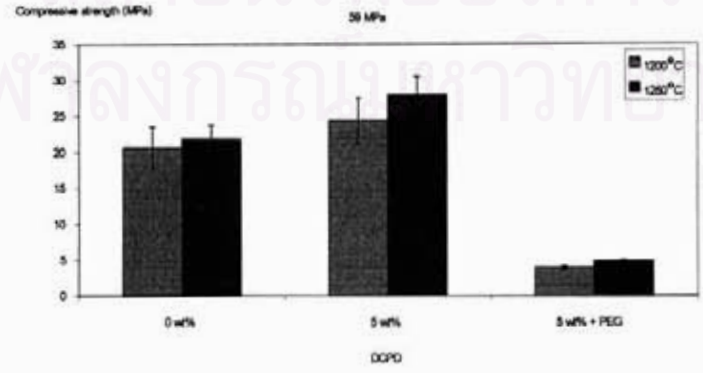

Fig. 4.28 Effect of sintering temperature on the compressive strength of specimens prepared from DCPD.

From the results of Table 4.2 and 4.3, with the exception of the flexural strength of DCPD specimens with glass addition, it can be said that the values of compressive and flexural strengths of the specimens well conform with their densities. Conflict in the mentioned case may be due to the big pores and TCP phases found in the glass containing specimens. The summarized results also clearly show that specimens prepared from DCPA have superior physical and mechanical properties, and all specimens containing PEG granules show very low strength which is due to their macropores. Results of Fig.4.25-4.28 indicate that glass does not effectively increase the flexural strength of the specimens sintered at 1200°C as it does in the case of compressive strength. However, the increase of strengths due to glass addition is not as big as expected. Raising the sintering temperature to 1250°C could increase both the flexural and compressive strengths of the DCPD specimens without glass, especially the flexural strength, close to that of the DCPA specimens without glass sintered at 1200°C. These findings had turned the research direction towards the improvement of the strengths of the specimens sintered at 1200°C by increasing pressing pressure. The effect of pressing pressure on the strengths of the specimens is presented in Table 4.4-4.5 and graphically illustrated in Fig. 4.29-4.30.

Table 4.4 Summarized results of physical properties and flexural strength of specimens (0 wt% glass) prepared from DCPD/DCPA at various pressing pressure.

Sintering temp. (1200°C)	DCPD			DCPA		
Pressing pressure	50.1 MPa	66.8 MPa	83.5 MPa	50.1 MPa	66.8 MPa	83.5 MPa
Bulk density (g/cm^3)	1.60	1.62	1.67	1.80	1.84	1.86
Apparent porosity (%V)	47.35	47.05	45.15	39.87	38.51	37.35
Flexural strength* (MPa)	8.36±0.36	8.74±1.23	9.78±0.20	15.32±1.72	16.96±0.59	17.51±1.77

* Number of specimens = 5, tested at 95% confidence level.

Table 4.5 Summarized results of physical properties and compressive strength of specimens (0 wt% glass) prepared from DCPD/DCPA at various pressing pressure.

Sintering temp. (1200°C)	DCPD		DCPA	
Pressing pressure	59 MPa	118 MPa	59 MPa	118 MPa
Bulk density (g/cm^3)	1.57	1.67	1.86	1.92
Apparent porosity (%V)	48.90	44.86	36.57	32.59
Compressive strength* (MPa)	20.59±2.89	26.09±3.38	64.88±5.02	78.13±10.37

* Number of specimens = 5, tested at 95% confidence level.

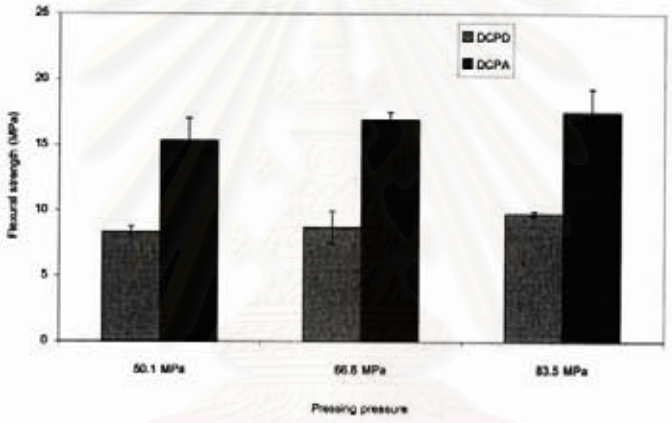

Fig. 4.29 Effect of pressing pressure on the flexural strength of specimens prepared from DCPD and DCPA.

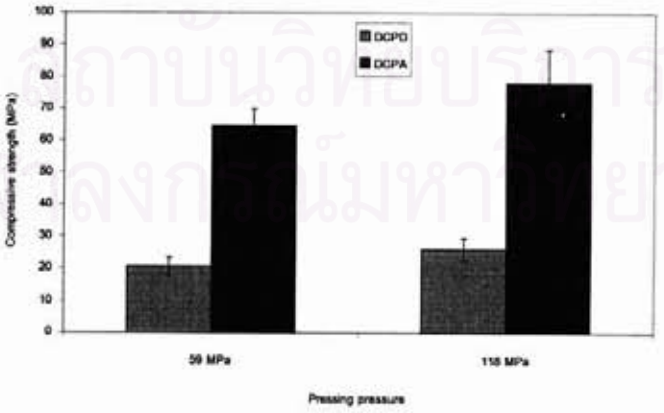

Fig. 4.30 Effect of pressing pressure on the compressive strength of specimens prepared from DCPD and DCPA.

It is found that the strengths of the specimens increase with increasing pressing pressure. The maximum flexural strength, 17.51 MPa, is obtained with DCPA specimens at 83.5 MPa pressing pressure, and the maximum compressive strength, 78.13 MPa, at 118 MPa pressing pressure. These values are ranged in the upper end reported for porous HA[12].

- Phase analysis

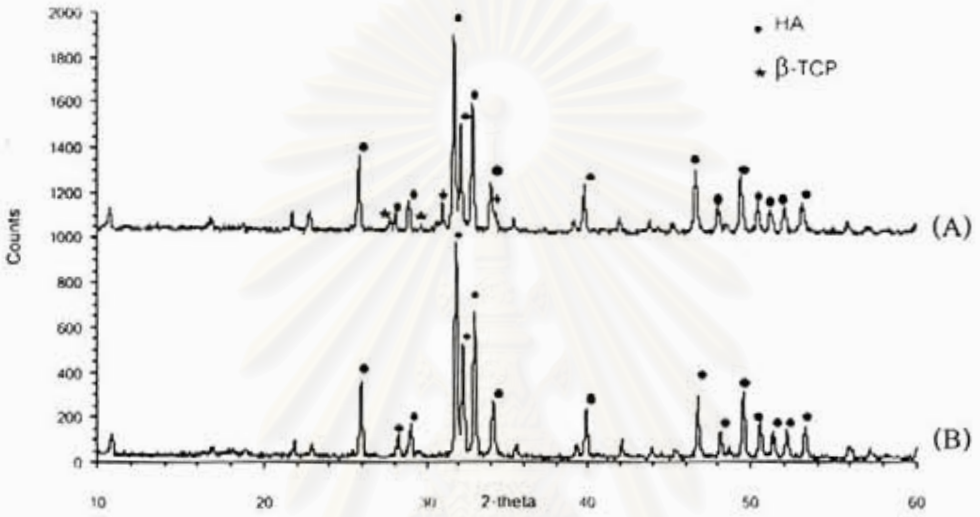

Fig. 4.31 XRD patterns of DCPA specimens sintered at 1200°C (pressing pressure 50.1 MPa) (A) 5 wt% $Ca(PO_3)_2$ (B) 0 wt% $Ca(PO_3)_2$.

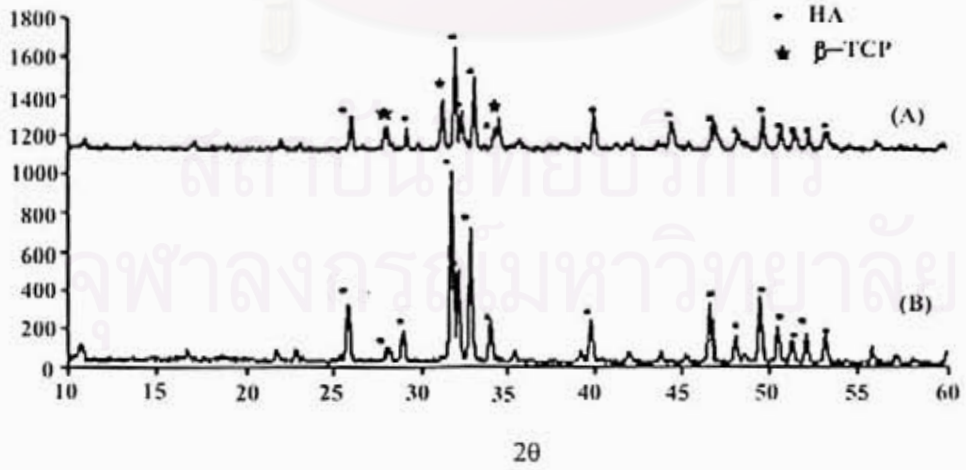

Fig. 4.32 XRD patterns of DCPD specimens sintered at 1200°C (pressing pressure 50.1 MPa) (A) 5 wt% $Ca(PO_3)_2$ (B) 0 wt% $Ca(PO_3)_2$.

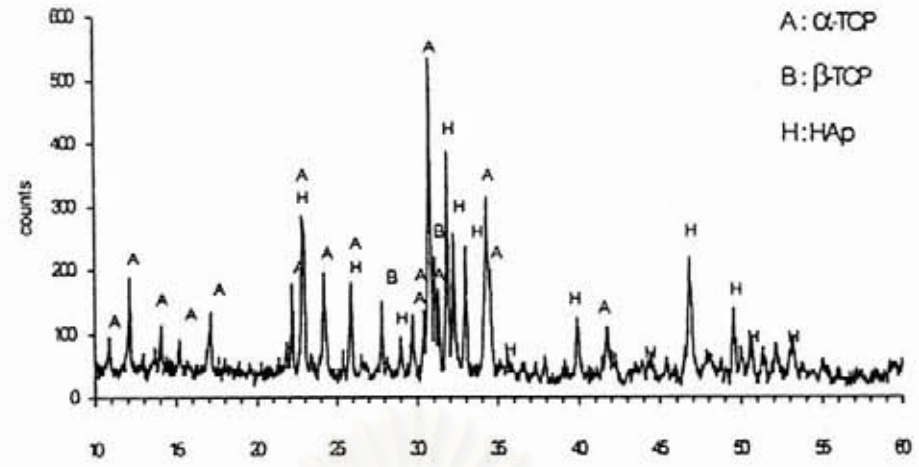

(A)

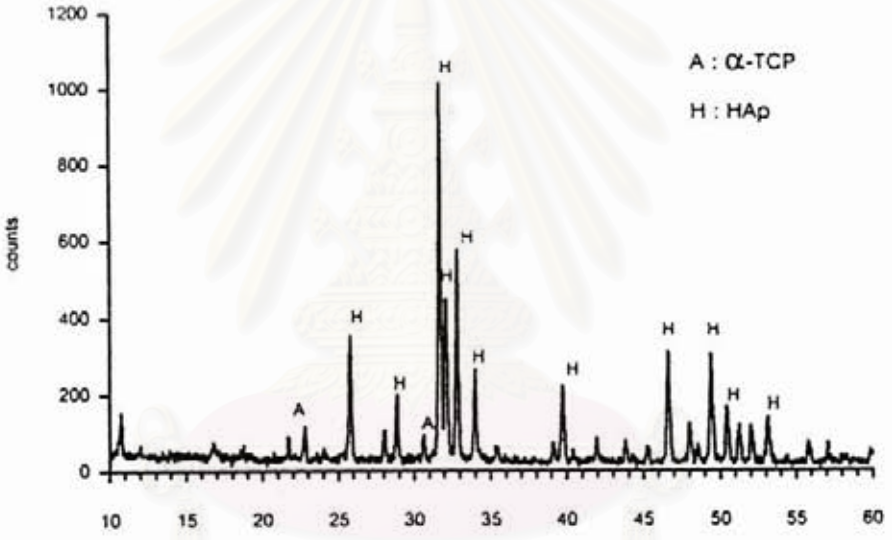

(B)

Fig. 4.33 XRD patterns of DCPD specimens sintered at 1250°C

(A) 5 wt% $Ca(PO_3)_2$,(B) 0 wt% $Ca(PO_3)_2$.

Fig. 4.31-4.33 show the XRD patterns of specimens prepared from DCPD and DCPA fabricated under different conditions. A single phase of HA is obtained for DCPD and DCPA specimens without glass addition sintered at 1200°C, and a trace of β-TCP is revealed as the 2 nd phase in all the specimens with glass. In the case of DCPD specimens without glass sintered at higher temperature, a trace of α -TCP is detected, and in the ones with

glass, a large amount of α-TCP is found in addition to a trace of β-TCP. Knowles[15] had reported that glass promoted the transition of HA to TCP and the process was accelerated with increasing temperature and glass content. Due to its low density, the extent of TCP, especially α-TCP, became critical to the strength of specimens.

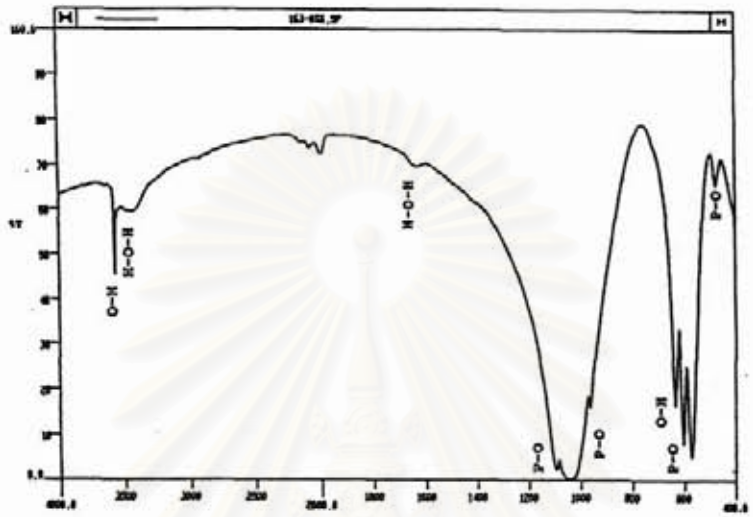

Fig. 4.34 FT-IR spectrum of DCPD, 0 wt% $Ca(PO_3)_2$, 1200°C.

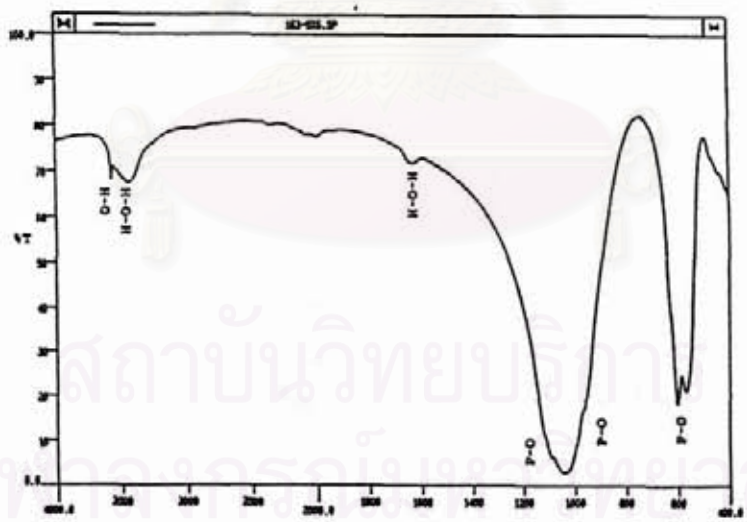

Fig. 4.35 FT-IR spectrum of DCPD, 5 wt% $Ca(PO_3)_2$, 1250°C.

The results of FT-IR, Fig. 4.34 and 4.35 well correspond to those of the XRD, i.e. only well crystallized HA phase is detected in the spectra of DCPD and DCPA with 0 wt % glass

samples sintered at 1200°C and the presence of TCP is detected in the spectra of DCPD and DCPA with 0.5 wt % glass samples sintered at 1200 and 1250°C, respectively.

- Microstructure

SEM micrgraphs of specimens from DCPD and DCPA fabricated under different conditions are shown in Fig. 4.36-4.38.

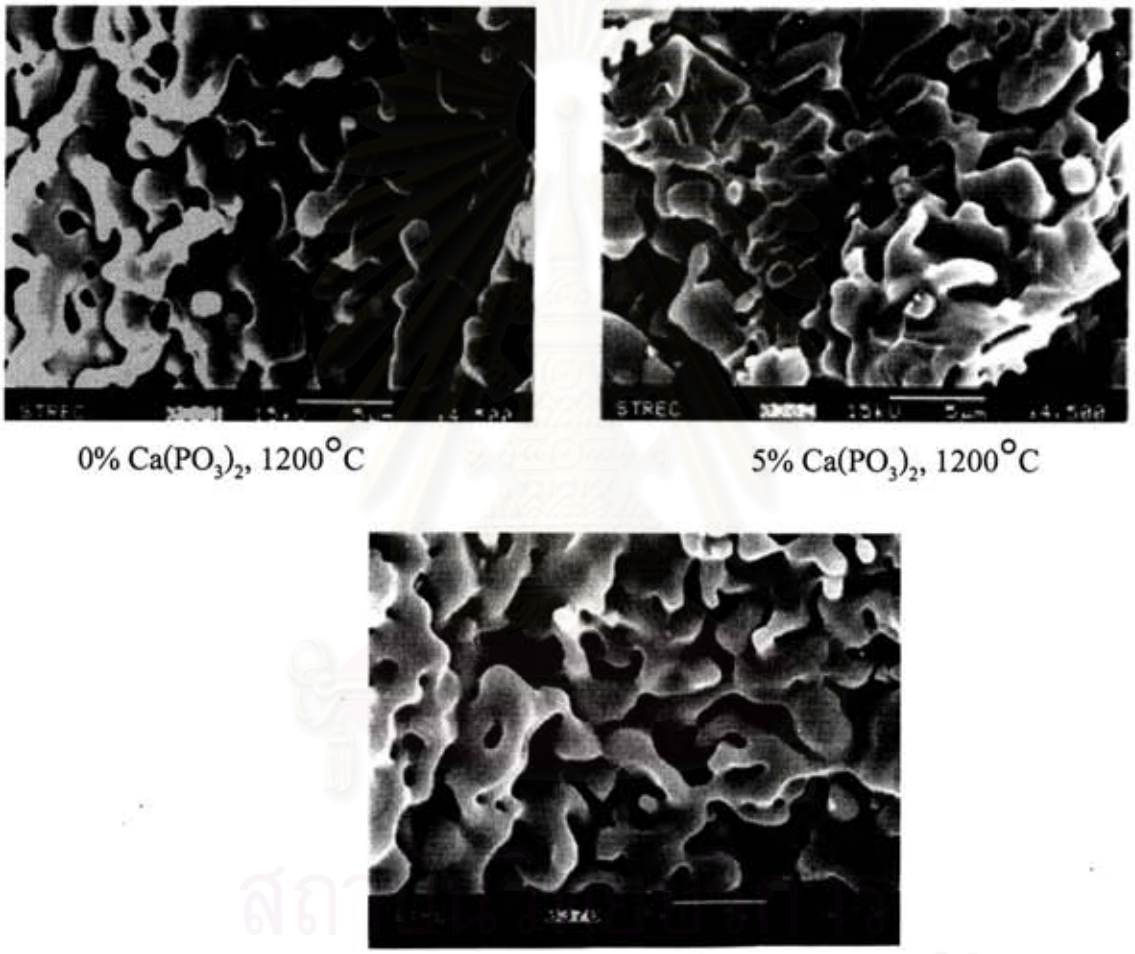

0% $Ca(PO_3)_2$, 1200°C

5% $Ca(PO_3)_2$, 1200°C

5% $Ca(PO_3)_2$, 1250°C

Fig. 4.36 Effect of glass and temperature upon the microstructures of DCPD specimens.

Fig. 4.36 reveals the interconnected micropores created by the adjacent grains necking with each other in the sintering process and the addition of glass as well as the increase in sintering temperature enhance densification.

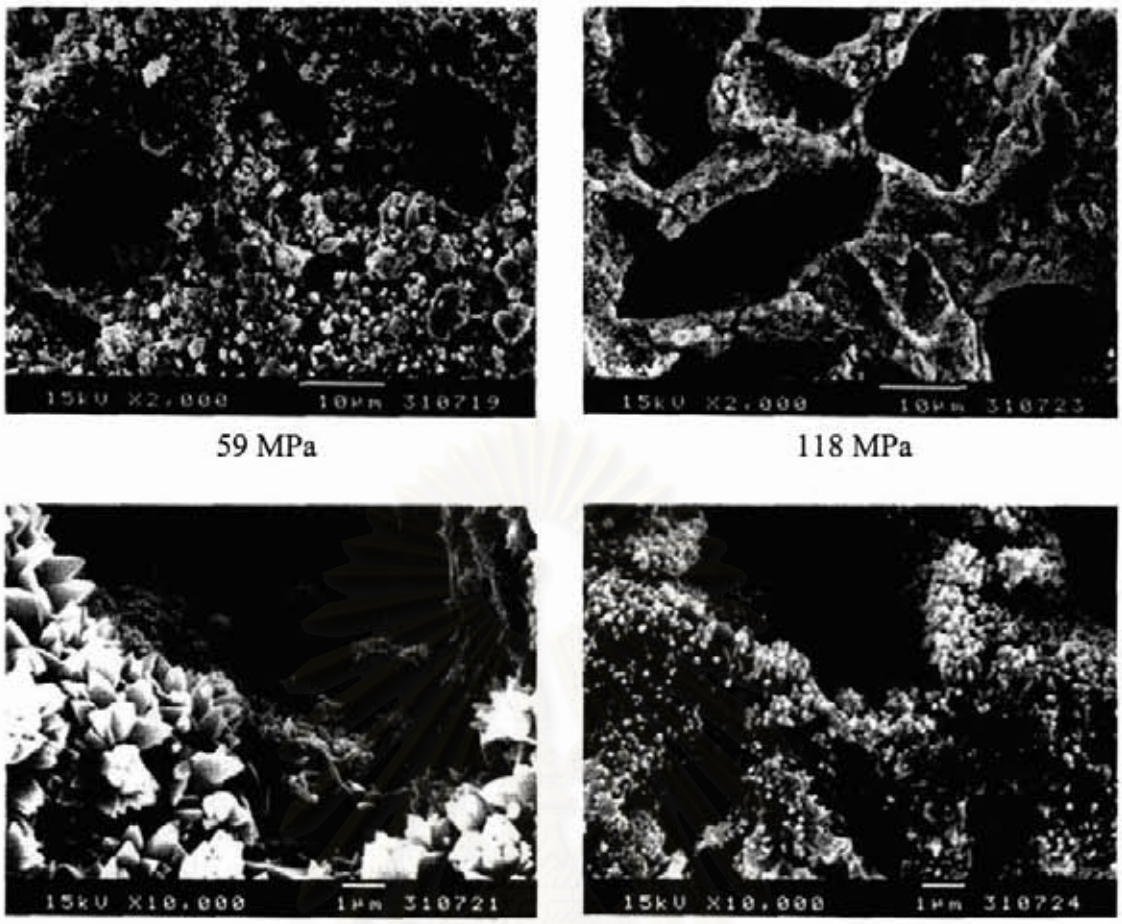

59 MPa 118 MPa

59 MPa 118 MPa

Fig. 4.37 Effect of pressing pressure upon the microstructures of DCPA specimens sintered at 1200°C.

The microstructures of Fig. 4.37 clearly show that the effect of green density on the microstructure of sintered specimens can be explained from the great reduction in microporosity and the morphology of the constituent crystal phase. The needle-like HA crystals of DCPA specimen pressed at 118 MPa are much smaller than those of the one at 59 MPa therefore it has denser microstructure, hence displays higher strength. Moreover it is noticed that the increase in pressure affects the shape but not the size of mesopores which is presumably created by the decomposition of $CaCO_3$ (median size 24 μm).

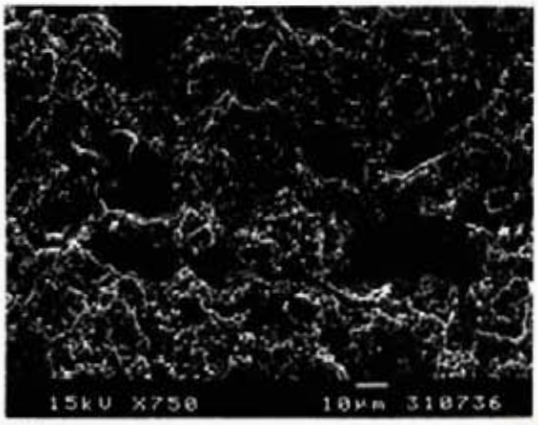

(a) DCPD flexural strength, 83.5 MPa

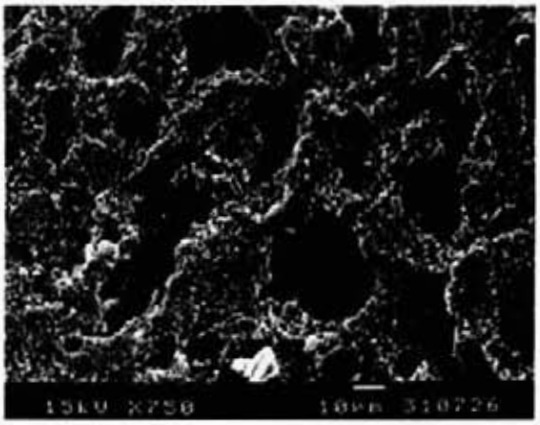

(b) DCPA flexural strength, 83.5 MPa

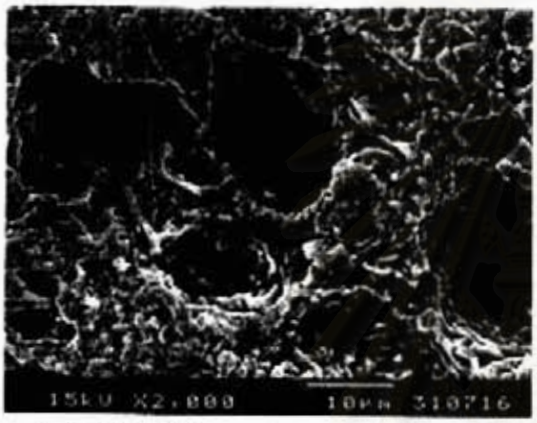

(c) DCPA flexural strength, 83.5 MPa

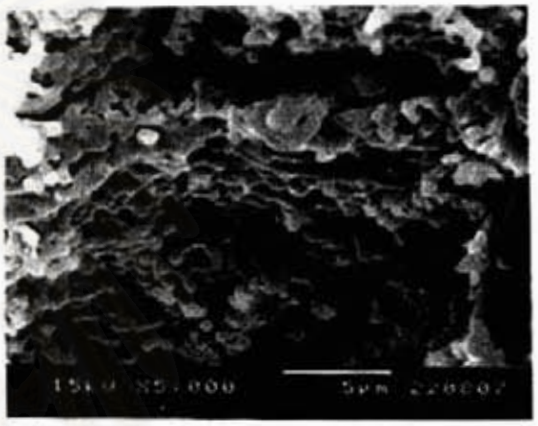

(d) DCPA flexural strength, 83.5 MPa

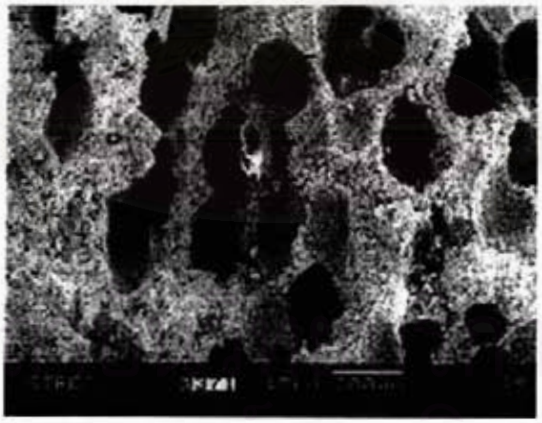

(e) DCPD + PEG granules + 5 wt% glass

Fig. 4.38 Microstructures of DCPA and DCPD specimens sintered at 1200°C, showing shapes and sizes of pores (micro and mesopores, a-c ; micropore enlarged, d).

The microstructures of Fig.4.38 (a-d) showing the size and shape of micropores (~1-5 μm) and mesopores (10-30 μm) of DCPD and DCPA specimens without glass addition

sintered at 1200°C, clearly confirm that the microstructure of DCPA specimen is denser than that of the DCPD specimen. Dense microstructure confines the release of CO_2 gas which consequently leads to a round and well-defined mesopores. Fig.4.38 (e), microstructure of DCPD specimen with PEG granules (150-300 μm) shows macropores (200 μm) created by the burning out of PEG granules.

4.2.3. Coralline hydroxyapatite

Corals have been known as a natural source of $CaCO_3$ and they are classified into many species. The ones that are appropriate for use as osteoconductive biomaterial should have the right pore size. Among these, coral of genus Porites having the average pore diameter of 200 μm is suitable and also available in the country. In this experiment, coral, the aragonite polymorph of $CaCO_3$ (Fig. 4.39) was hydrothermally treated with a phosphate solution in a teflon-lining, pressurized steel bomb at 200 °C. The inside pressure was self-generated by the water vapour. Aragonite was described as pseudohexagonal (a = 9.39 A°, c = 5.74 A°, γ = 117°) with similar lattice parameters, ionic position and ionic contents to HA (hexagonal, a = 9.43 A°, c = 6.88 A°, γ = 120 °). Accordingly, the aragonite-HA conversion was characterized as a topotactic ion exchange reaction[17]. The detail of experiment is presented as a flow chart in Fig. 3.2. After a series of attempt, the typical conditions were selected and the summarized results are listed in Table 4.6.

Table 4.6 Summarized results of aragonite-hydroxyapatite hydrothermal conversion.

Material	h	Ca/P	Temperature (°C)	pH		phase obtained
				Before	after	
MCPM + coral + $Ca(OH)_2$	14	1.67	200	2.8	3.8	HA + DCPA + aragonite + calcite*
DCPA + coral + $Ca(OH)_2$	14	1.67	200	2.9	2.8	HA + DCPA + aragonite + calcite*

*$CaCO_3$ in the form of calcite caused by atmospheric CO_2 reacted with $Ca(OH)_2$.

Fig. 4.40-4.41 are the XRD and SEM results of the products obtained under various conditions.

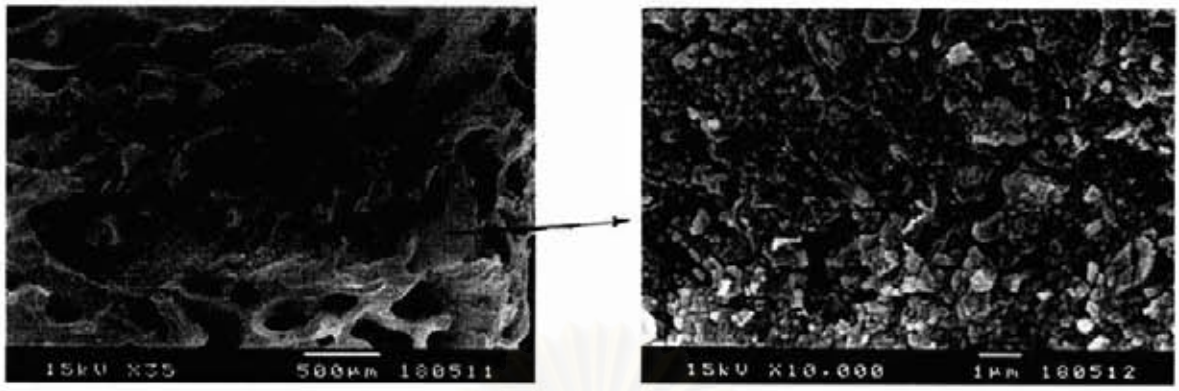

(a) (b)

Fig. 4.39 SEM micrographs of Porites coral.

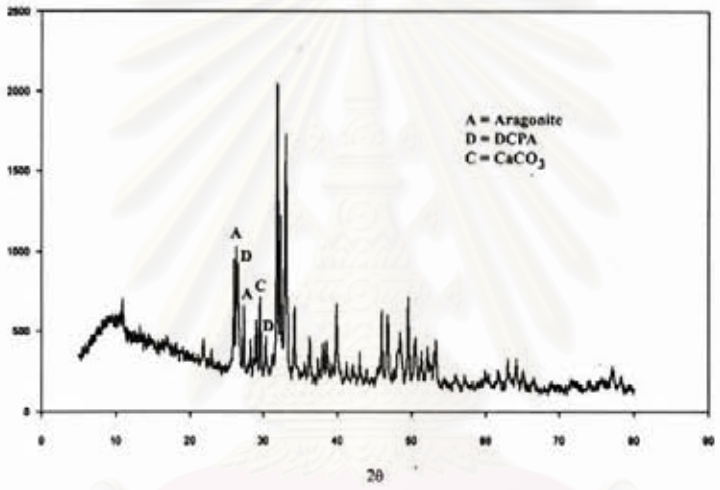

Fig. 4.40 XRD patterns of hydrothermal products.

(coral + MCPM + $Ca(OH)_2$, 200°C, 14 h)

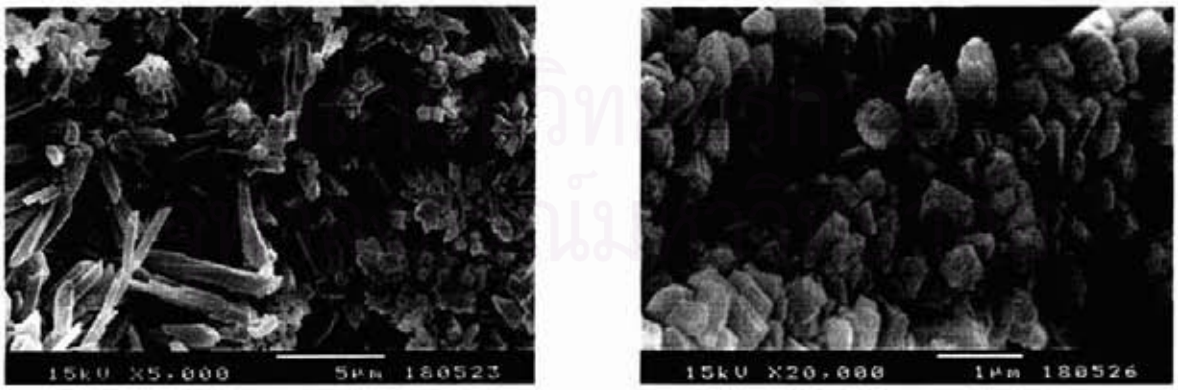

(a) (b)

Fig. 4.41 SEM micrographs of hydrothermal products.

(DCPA + coral + $Ca(OH)_2$, 200°C, 8 h)

The results of XRD reveal that the main phase obtained is HA and the rest are traces of aragonite and DCPA. The SEM micrographs show rod-shaped crystals of HA growing at the expense of DCPA tablets and whiskers which serve as an intermediate phase in the transformation of $CaCO_3$ to HA[18].

The reactions taking place are suggested as follows:

$$CaCO_3 + H_2PO_4^- + H^+ \rightarrow CaHPO_4 + H_2O + CO_2 \quad (\text{pH}\sim 2\text{-}4)$$

$$6CaHPO_4 + 4Ca(OH)_2 \rightarrow Ca_{10}(PO4)_6(OH)_2 + 6H_2O \quad (\text{pH}\sim 6\text{-}12).$$

Chapter 5

Conclusion

Since there are several fabrication techniques have been attempted, for simplicity,their conclusions will be drawn separately as follows:

Porous granules: Granules (diameter ~ 300-500 μm) containing the single phase of HA have been successfully produced by granulation of either DCPA or DCPD with $CaCO_3$ powders and sintering at 1200 °C in air.

Porous specimens : The sintered porous specimens, obtained from casting the slip of DCPA or DCPD with $CaCO_3$ in the presence of H_2O_2 as foaming agent contain mixed phases of HA, CaO and β-TCP due to segregation of slip composition, so they do not display a high strength. The porous specimens containing the single phase of HA have been successfully produced from pressing DCPA or DCPD with $CaCO_3$ and sintering at 1200-1250°C. The maximum flexural and compressive strengths obtained are 17.51 MPa and 78.13 MPa from DCPA + $CaCO_3$ specimens sintered at 1200°C which are considered to be in the upper range reported for porous HA.

Coralline HA : Porites coral skeleton has been successfully converted hydrothermally to HAp of which only traces of aragonite and DCPA are detected. After the conversion, the original pore size of the coral was retained and the coral skeleton remained intact.

Future suggestion

The following researches are going to be performed in order to follow the consequence of the application.

1. In vivo study on compatibility of the sintered compacts and granules.
2. Plasma spray coating of green DCPD or DCPA granules on Ti alloy.

References

1. Jinawath, S. and Trakarnvichit, S., Preparation of Calcium Phosphate Dihydrate from Cattle Bone. 2nd International Symposium on Apatite, Tokyo, Vol. 12 (1997), 48-52.
2. Limpanuphap, S., Preparation of Calcium Phosphate Compounds from By-Product of Bone-Gelatin Production, M.S. Thesis (ceramic technology,1999), Chulalongkorn University.
3. Shareef, M.Y. and Messer, P.F., Fabrication, characterization and fracture study of a machinable hydroxyapatite ceramic, Biomaterials (1993), 14[1] 69-75.
4. Arita, I.H., et al., Chemistry and sintering behaviour of thin hydroxyapatite ceramics with controlled porosity, Biomaterials, Vol. 11, No. 5 (1995) : 403-406.
5. Faberri, M., Celotti, G.C. and Ravaglioli, A., Granulates based on calcium phosphate with controlled morphology and porosity for medical applications : physio-chemical parameters and production technique, Biomaterials, 15[6] (1994), 474-477.
6. Aoki, H. Medical Applications of Hydroxyapatite. Takayama Press System Center Co., Inc., Japan, 1994.
7. LeGeros,R.Z., Calcium Phosphate Materials in Restorative Dentistry : A Review. Adv.Dent.Res. 2(1) (1998) : 164-180.
8. LeGeros, R.Z., Calcium Phosphate in Oral Biology and Medicine. Monographs in Oral Science: Vol. 15, KARGER, Basel, Switzerland, 1991.
9. Hench, L.L., Bioceramic, J. Am. Ceram. Soc., 81 [1] (1998) : 1705-28.
10. Supulveda, P., Gelcasting foams for porous ceramics, Am. Ceram. Soc. Bull. 76[10]. Nov (1997) : 61-65.
11. Liu, D. M., Preparation and characterization of porous hydroxyapatite bioceramic via a slip-casting route, Ceramic International, 24 (1998) : 441-446.
12. Suchanek, W., and Yoshimura, M., Processing and properties of hydroxyapatite-based biomaterial for use as hard tissue replacement implants, J. Mater. Res., Vol. 13, No.1 Jan (1998) : 94-117.

13. Reed, J.S., Principles of ceramic processing 3rd ed. N.Y., John Wiley & Sons, 1995.

14. Onoda, G., Paper presented at the 97th Annual Meeting of the American Ceramic Society, Cincinati, O.H., 1995.

15. Knowles, J.C., and Bonfield, W. Development of glass reinforced hydroxyapatite with enhance mechanical properties and its relationship to phase changes., J. Biomed. Mat. Res. Vol. 27 (1993) : 1591-1598.

16. Kondo, K., et al., Preparation of high-strength apatite ceramics., Communication of the American Ceramic Society., Nov (1984) : C222-C223.

17. Zaremba, C. M., Morse, D. E., Mann, S., Hansma, P. K., and Stucky, G. D., Aragonite-hydroxyapatite conversion in gastropod (abalone) nacre, Chem. Mater., Vol. 10, No.12 (1998) : 3813-24.

18. Jinawath, S., Hydrothermal synthesis of hydroxyapatite from natural source, Paper presented at the conference, SSP-2000, Tokyo, Dec. 11-13 (2000).